Higher-order derivatives of the Green function in hyper-singular integral equations

Liang, Hui; Shao, Yanlin; Chen, Jikang

Published in:
European Journal of Mechanics B - Fluids

Link to article, DOI:
10.1016/j.euromechflu.2020.12.006

Publication date:
2021

Document Version
Peer reviewed version

Higher-order derivatives of the Green function in hyper-singular integral equations

Hui Liang[a], Yanlin Shao[b,c], Jikang Chen[c,*]

[a] *Technology Centre for Offshore and Marine, Singapore (TCOMS), 118411, Singapore*
[b] *Department of Mechanical Engineering, Technical University of Denmark, 2800 Lyngby, Denmark*
[c] *College of Shipbuilding Engineering, Harbin Engineering University, Harbin, 150001, China*

Abstract

Hyper-singular integral equations are often applied in the frequency-domain wave diffraction/radiation analyses of marine structures with thin plate or shell sub-structures. Their numerical solutions require the second-order derivatives of the free-surface Green function featuring hyper-singularity, and hence the corresponding evaluation is very challenging. To circumvent the associated numerical difficulties, this paper will propose alternative formulations for the higher-order derivatives of both free-surface and Rankine-source parts of the Green function. For the free-surface term G^F, the higher-order derivatives are analytically expressed by a combination of G^F itself and its first-order horizontal radial derivative. Further, we derive an asymptotic representation, enabling us to deal exactly with a removable singularity in this representation. The superiority of the proposed formulation is demonstrated by comparing with a conventional direct differentiation. For the Rankine-source term, analytical expressions for the velocities induced by a uniform dipole distribution over a flat panel (involving second derivatives of the Rankine source term) are presented, which is directly relevant for numerical implementation based on constant panel methods. As illustrative examples, linear hydrodynamic coefficients of submerged circular impermeable and perforated plates are calculated for verification purposes. The proposed formulas are simple and easy to implement in the hyper-singular integral equations.

Keywords: Green function, Second derivative, Wave diffraction/radiation, Hyper-singular integral equation

1. Introduction

Most of the marine structures feature large volume. Therefore, it is often reasonable to use the potential-flow theory to predict the loading and response of these structures. Viscous forces are generally of secondary importance for large-volume structures and thus can be accounted for empirically [1, 2]. The combination of the potential-flow theory and viscous correction has proven to be useful and efficient in the design and analysis of marine structures.

Diffraction/radiation analysis of regular waves in the frequency domain are often carried out in offshore engineering to determine the hydrodynamic coefficients, including: added mass, wave-radiation damping, wave exciting forces and pressure distribution, which can be used as input in the design of marine structures and their station-keeping systems [1, 2]. The more powerful time-domain analysis based on Cummins equations [3, 4] also needs the frequency-domain hydrodynamic coefficients as inputs.

The application of boundary element methods (BEMs) in solving the frequency-domain linear diffraction/radiation problems has been seen as a great success in marine hydrodynamics. The free-surface Green function, representing the velocity potential due to a time-harmonically pulsating source beneath or at a free surface, and satisfying the linearised free-surface boundary conditions and radiation condition in the far field [5], is widely adopted as the fundamental solution in the solution of the Laplace equation. The Green function consists of two parts, namely the free-surface term G^F and the Rankine-source term.

In light of its importance, efficient and accurate evaluation of the Green function has been extensively studied in the literature. In summary, the evaluation of the Green function can be categorized into:

1. Approximations within complementary contiguous flow regions [6, 7, 8, 9, 10]
2. Global approximation valid within the entire flow region [11, 12, 13]
3. Table interpolation with the utilisation of coordinate transformation [14, 15]
4. Solving ordinary differential equation [16, 17, 18]

The accuracy and time-efficiency of different algorithms have been commented in a recent review by Xie *et al.* [19]. Usually, the focus is placed on the Green function itself, whereas the derivatives are evaluated via straightforwardly differentiating the expressions of approximation. For the evaluation of derivatives, more terms are needed to ensure the same level of accuracy [19].

Thin plates are often used in marine and offshore engineering as economical and efficient damping devices to provide extra damping through viscous flow separation at sharp edges. They can also provide extra inertia to the floating system, which may be beneficial from design point of view to avoid possible motion resonances. Examples of

*Corresponding author
Email address: liang_hui@tcoms.sg (Hui Liang); yshao@mek.dtu.dk (Yanlin Shao); cjkhrb@sina.com (Jikang Chen) (Jikang Chen)

those devices are the heave plate in Spar platforms, the bottom flanges in cylindrical floating production storage and offloading (FPSO) units [20] and floating pontoon in sea-crossing bridge designs [21, 22]. In hydrodynamic analysis based on BEMs, thin plates are often mathematically modelled as zero-thickness structures, which leads to hyper-singular boundary integral equations (BIEs) involving second derivatives of the Green function [23]. In principle, one may also model the thin plate as a finite-thickness plate to avoid hyper-singular BIEs, which however requires distribution of singularities on all surfaces of the plate, thus may unnecessarily increase the number of unknowns and computational costs. Similarly, modelling of a dissipation surface by a perforated plate [24, 25, 26] and shell structures [27, 28] as well as the application of enhanced overdetermined integral equations for irregular frequencies removal [29] and the computation of velocities in the fluid domain by means of a combined source-dipole distribution also involve the solution of hyper-singular BIEs.

Despite its importance, accurate evaluation of higher-order derivatives of the Green function has not been thoroughly discussed in the literature. Theoretically, higher-order derivatives of the free-surface term G^F in the Green function can be evaluated by differentiating the existing expressions of the approximation. However, direct differentiation will drastically reduce the accuracy of the evaluation. To achieve a given level of accuracy, many expansion terms may be required in the evaluation of the higher-order derivatives. It means that additional coefficients for polynomial interpolation or other types of approximation must be generated, thus complicating the implementation. In addition, higher-order derivatives of G^F are difficult to evaluate if the highly-efficient global approximations given in [11, 12, 13] are used. The integration of higher-order derivatives of the Rankine-source term is also tremendously difficult. The challenge is related to the calculation of velocity components induced by a dipole distribution over a panel.

The present paper aims at circumventing the numerical difficulties associated with the second derivatives of Green function in the three-dimensional hyper-singular integral equations [25, 26, 23]. To achieve that, alternative formulations for the second derivatives of both the free-surface and Rankine-source terms in the Green function will be presented. For the free-surface term G^F, analytical expressions of the second derivative of G^F are derived. It is shown that all the second derivatives can be expressed by means of G^F and its horizontal radial derivative G^F_h, and thus can be evaluated without extra effort. Generalization to even higher-order derivatives is straightforward. Special attention will be paid to the cases where the horizontal radial distance between the source point and field point (denoted as h hereafter) asymptotically approaches zero, since the second derivatives of G^F take a zero-over-zero form. Analysing the asymptotic representation also enables us to deal exactly with this removable singularity when $h \to 0$. For the Rankine-source term in the Green function, analytical expressions for the velocities induced by a uniform dipole distribution over a flat panel (involving second derivatives of the Rankine source term) will also be presented. They are immediately useful for numerical implementation based on the constant panel method.

The present paper is organized as follows: The mathematical formulation of the hyper-singular BIEs, notation and basic definitions are presented in Sect. 2. In Sect. 3, the second derivatives of the free-surface term G^F are formulated. Sect. 4 presents asymptotic results for the second derivatives of G^F when $h \to 0$. The superiority of the proposed formulations over the conventional direct differentiation is demonstrated in Sect. 5. The alternative formulation to evaluate the velocity components induced by a uniform dipole distribution over a flat panel is presented in Sect. 6. In Sect. 7, the diffraction/radiation of regular waves by submerged solid and perforated circular discs are studied to verify the formulations presented in this paper. Finally, concluding remarks are presented in Sect. 8.

2. Definitions and hyper-singular boundary integral equations

A Cartesian system of coordinates $\boldsymbol{X} \equiv (X, Y, Z)$ is defined. The Z axis is vertical and points upward, and the undisturbed free surface is taken as the plane $Z = 0$. Deep water is assumed, and the diffraction/radiation of time harmonic waves with the radian frequency ω and wavelength $\lambda = 2\pi g/\omega^2$ is considered. Here g denotes the gravitational acceleration. We define non-dimensional coordinates as

$$\boldsymbol{x} \equiv (x, y, z) \equiv (X, Y, Z)\,\omega^2/g. \tag{1}$$

The Green function $G(\boldsymbol{x}, \boldsymbol{\xi})$ corresponds to the spatial component of a non-dimensional velocity potential

$$\Psi(\boldsymbol{x}, \boldsymbol{\xi}, T) = \mathrm{Re}[G(\boldsymbol{x}, \boldsymbol{\xi})\mathrm{e}^{-\mathrm{i}\omega T}], \tag{2}$$

where T denotes time. Expression (2) represents the potential of the flow created at the flow-field point $\boldsymbol{x} \equiv (x, y, z \le 0)$ by a pulsating source located at the point $\boldsymbol{\xi} \equiv (\xi, \eta, \zeta < 0)$, or by a flux through the free surface at the point $\boldsymbol{\xi} \equiv (\xi, \eta, \zeta = 0)$.

As illustrated in Fig. 1, the non-dimensional distances between the flow-field point $\boldsymbol{x}$ and the source point $\boldsymbol{\xi}$ or its mirror image $\boldsymbol{\xi}^M \equiv (\xi, \eta, -\zeta)$ with respect to the undisturbed free-surface plane $z = 0$ are denoted as r and d, respectively. They are defined as

$$r \equiv \sqrt{(x-\xi)^2 + (y-\eta)^2 + (z-\zeta)^2}, \tag{3a}$$

$$d \equiv \sqrt{(x-\xi)^2 + (y-\eta)^2 + (z+\zeta)^2}. \tag{3b}$$

The horizontal and vertical components of the distance d between the points $\boldsymbol{x}$ and $\boldsymbol{\xi}^M$ are given by

$$0 \le h \equiv \sqrt{(x-\xi)^2 + (y-\eta)^2} \quad \text{and} \quad v \equiv z + \zeta \le 0. \tag{4}$$

For an infinite-thin plate or a shell sub-structure, the BIE which is a result of applying Green's third identity to the Laplace equation in the fluid domain, is expressed as [30]:

$$-\frac{1}{4\pi}\iint_S [\phi(\boldsymbol{\xi})]\frac{\partial^2 G(\boldsymbol{x}, \boldsymbol{\xi})}{\partial n_{\boldsymbol{x}} \partial n_{\boldsymbol{\xi}}}\mathrm{d}S = V_n(\boldsymbol{x}), \tag{5}$$

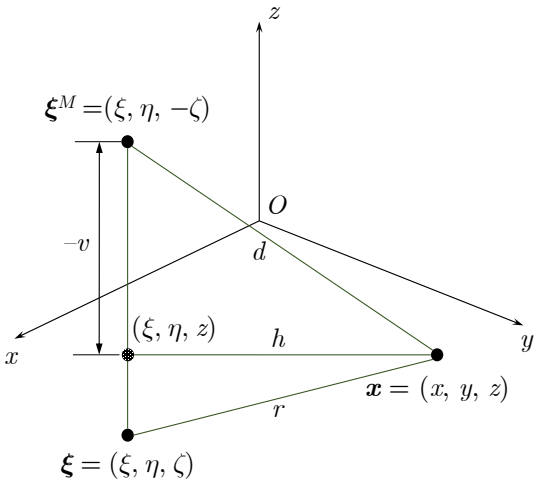

Figure 1: Sketch of definition.

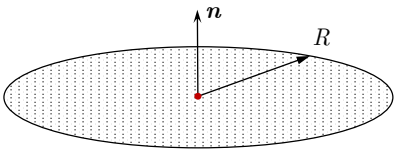

Figure 2: Sketch of a circular disc.

where S is either the upper or lower part of the plate surface. Another application is the computation of velocities in the fluid domain when a combined source-dipole distribution is applied, and the corresponding integral equation is expressed as:

$$\nabla_{\boldsymbol{x}}\phi(\boldsymbol{x}) = \frac{1}{4\pi}\iint_S \nabla_{\boldsymbol{x}}\left[V_n(\boldsymbol{\xi})G(\boldsymbol{x},\boldsymbol{\xi}) - \phi(\boldsymbol{\xi})\frac{\partial G(\boldsymbol{x},\boldsymbol{\xi})}{\partial n_{\boldsymbol{\xi}}}\right]\mathrm{d}S. \tag{6}$$

Here the Green function $G(\boldsymbol{x},\boldsymbol{\xi})$ has been chosen so that $\mathrm{Re}[G(\boldsymbol{x},\boldsymbol{\xi})\mathrm{e}^{-\mathrm{i}\omega T}]$ satisfies the combined linearised free surface condition and the radiation conditions in the far field. More details for $G(\boldsymbol{x},\boldsymbol{\xi})$ and its derivatives will be given in Sect. 3. V_n is the normal velocity at the structure surface associated with the body boundary condition, and $[\phi(\boldsymbol{\xi})]$ is defined as $[\phi(\boldsymbol{\xi})] = \phi^+(\boldsymbol{\xi}) - \phi^-(\boldsymbol{\xi})$ with superscripts $\pm$ denoting the upper and lower sides of the plate, respectively. $\boldsymbol{n}_{\boldsymbol{x}}$ and $\boldsymbol{n}_{\boldsymbol{\xi}}$ are the normal vectors at the flow-field and singularity points on the structure surface. For a structure of non-zero displacement, the normal vector is defined positive pointing into the fluid domain. When a horizontal plate is considered, the normal vector points positively upward as illustrated in Fig. 2. The hyper-singular integral equations (5) and (6) indicate that the evaluation of second derivatives of the Green function is required when infinite-thin plates are considered or velocities in the fluid domain are calculated.

3. Green function and derivatives

The free-surface Green function for the wave diffraction/radiation analysis of marine structures is expressed as [5]

$$G = -\frac{1}{r} - \frac{1}{d} + G^F. \tag{7}$$

Here G^F is the free-surface term in the Green function, which represents the velocity potential due to the free-surface disturbance

$$G^F(h,v) = -2\int_0^\infty \frac{1}{k-1}\mathrm{e}^{kv}J_0(kh)\mathrm{d}k, \tag{8}$$

where $J_0(\cdot)$ is the zeroth-order Bessel function of the first kind [31], and the integral is interpreted as bypassing the pole at $k=1$ from below to satisfy the radiation condition.

There is a lot of discussion in the literature on the evaluation of the free-surface term itself, thus will not be repeated here. The focus will be placed on the derivatives of G^F hereafter. By definition, the first derivatives can be expressed as

$$G^F_x = G^F_h\frac{x-\xi}{h}, \tag{9a}$$

$$G^F_y = G^F_h\frac{y-\eta}{h}, \tag{9b}$$

$$G^F_z = -\frac{2}{d} + G^F, \tag{9c}$$

and the second derivatives are expressed as

$$G^F_{xx} = G^F_{hh}\frac{(x-\xi)^2}{h^2} + G^F_h\frac{(y-\eta)^2}{h^3}, \tag{10a}$$

$$G^F_{xy} = G^F_{yx} = \left(G^F_{hh} - \frac{G^F_h}{h}\right)\frac{(x-\xi)(y-\eta)}{h^2}, \tag{10b}$$

$$G^F_{xz} = G^F_{zx} = G^F_{hv}\frac{x-\xi}{h}, \tag{10c}$$

$$G^F_{yy} = G^F_{hh}\frac{(y-\eta)^2}{h^2} + G^F_h\frac{(x-\xi)^2}{h^3}, \tag{10d}$$

$$G^F_{yz} = G^F_{zy} = G^F_{hv}\frac{y-\eta}{h}, \tag{10e}$$

$$G^F_{zz} = G^F_{vv}. \tag{10f}$$

By directly differentiating the integral expression (8), second derivatives G^F_{hh}, G^F_{hv} and G^F_{vv} can further be expressed as (see Appendix A for details)

$$G^F_{hh} = -\frac{2v}{d^3} + \frac{2}{d} - G^F - \frac{1}{h}G^F_h, \tag{11a}$$

$$G^F_{hv} = \frac{2h}{d^3} + G^F_h, \tag{11b}$$

$$G^F_{vv} = \frac{2v}{d^3} - \frac{2}{d} + G^F. \tag{11c}$$

Therefore, all the first and second derivatives can be represented by a combination of the Green function itself G^F and its radial derivative G^F_h, which have been extensively investigated in the literature. Even higher-order derivatives can also be expressed by a combination of G^F and G^F_h if needed.

Despite representations (10) and (11) present explicit formulations for the second derivatives of the Green function, special attention should be paid to the case $h=0$. The asymptotic analysis in [6] has shown $G^F_h(h=0,v) = 0$, and thus the last term $-G^F_h/h$ in (11a) is a zero-over-zero form limit.

4. Asymptotic behaviour as $h \to 0$

The asymptotic behaviour of the free-surface term G^F and its horizontal radial derivatives (G^F_h and G^F_{hh}) at $h = 0$ are considered. According to [6, 7], the Green function near the axis $h = 0$ can be expanded into a double infinite series

$$G^F = -2\sum_{n=0}^{\infty} \frac{(-h^2)^n}{4^n (n!)^2} I_n - 2\pi \mathrm{i} \mathrm{e}^v J_0(h), \tag{12a}$$

with I_n given by

$$I_n = \sum_{m=1}^{2n} \frac{(m-1)!}{(-v)^m} - \mathrm{e}^v \mathrm{Ei}(-v).$$

Expression (12a) can be applied to approximate the Green function G^F in the region $0 \le h/(-v) \le 0.5$ in which six digits of accuracy can be achieved with no more than 10 terms [19]. By differentiating (12a) with respect to h, the derivatives G^F_h and G^F_{hh} are written as

$$G^F_h = -2\sum_{n=1}^{\infty} \frac{2n}{h} \frac{(-h^2)^n}{4^n (n!)^2} I_n + 2\pi \mathrm{i} \mathrm{e}^v J_1(h), \tag{12b}$$

$$G^F_{hh} = \sum_{n=1}^{\infty} \frac{(2n^2 - n)(-h^2)^{n-1}}{4^{n-1} (n!)^2} I_n + 2\pi \mathrm{i} \mathrm{e}^v \left[J_0(h) - \frac{J_1(h)}{h} \right], \tag{12c}$$

where $\mathrm{Ei}(\cdot)$ means the exponential integral [31], which can be calculated in a straightforward manner. Then, the asymptotic expansions for a small h are

$$G^F = 2\mathrm{e}^v \mathrm{Ei}(-v) - 2\pi \mathrm{i} \mathrm{e}^v + O(h^2), \tag{13a}$$

$$G^F_h = h \left[\frac{1}{-v} + \frac{1}{(-v)^2} - \mathrm{e}^v \mathrm{Ei}(-v) + \pi \mathrm{i} \mathrm{e}^v \right] + O(h^3), \tag{13b}$$

$$G^F_{hh} = \frac{1}{-v} + \frac{1}{(-v)^2} - \mathrm{e}^v \mathrm{Ei}(-v) + \pi \mathrm{i} \mathrm{e}^v + O(h^2), \tag{13c}$$

where the expansions of Bessel functions $J_0(\cdot)$ and $J_1(\cdot)$ for a small argument [31] have been used. At $h = 0$, expressions (13) become

$$G^F(h = 0, v) = 2\mathrm{e}^v \mathrm{Ei}(-v) - 2\pi \mathrm{i} \mathrm{e}^v, \tag{14a}$$

$$G^F_h(h = 0, v) = 0, \tag{14b}$$

$$\lim_{h \to 0} \frac{G^F_h}{h} = \frac{1}{-v} + \frac{1}{(-v)^2} - \mathrm{e}^v \mathrm{Ei}(-v) + \pi \mathrm{i} \mathrm{e}^v, \tag{14c}$$

$$\begin{aligned} G^F_{hh} &= \frac{1}{-v} + \frac{1}{(-v)^2} - \mathrm{e}^v \mathrm{Ei}(-v) + \pi \mathrm{i} \mathrm{e}^v \\ &= \frac{1}{d} - \frac{v}{d^3} - \mathrm{e}^v \mathrm{Ei}(-v) + \pi \mathrm{i} \mathrm{e}^v. \end{aligned} \tag{14d}$$

For a vanishing horizontal distance between the source point and flow-field point ($h \to 0$), equations (14) should be used instead to deal with the zero-over-zero form limit, which is expected to be more accurate and efficient than a conventional direct differentiation approach.

5. Comparison with the direct differentiation

The comparison between a direct differentiation and the proposed formulation in Sect. 3 is made in this section, and two typical evaluations are considered.

In the region $0 \le h/(-v) \le 0.5$, the expressions (12a) and (12b) are widely used to evaluate G^F and G^F_h. To achieve a six-decimal accuracy for both G^F and G^F_h, the series are truncated with $n = 10$. Here, we compare the approximations to G^F_{hh} via the direct differentiation (12c) and the proposed formulation (11a) with the series truncated to $n = 10$. Fig. 3 depicts the errors due to two approximations to the real part of G^F_{hh}. It can be observed that the proposed formulation still keeps around a six-decimal accuracy, whereas the errors of results based on the direct differentiation are in general more than 10 times larger.

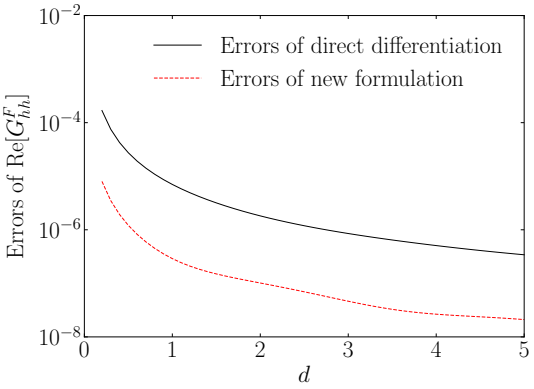

Figure 3: Errors of approximations of G^F_{hh} due to the direct differentiation and the proposed new formulation versus d for $h/(-v) = 0.5$.

Then, we consider another approximation widely adopted in the far field, and the approximation to G^F is written as [6]

$$G^F \approx 2\pi \mathrm{e}^v [Y_0(h) - \mathrm{i} J_0(h)] + 2\sum_{n=0}^{\infty} \mathscr{P}_n, \tag{15a}$$

where $\mathscr{P}_n$ are defined as

$$\mathscr{P}_n = \frac{\partial^n}{\partial v^n} \left(\frac{1}{d} \right) = \frac{P_n(\alpha)}{d^{n+1}}, \tag{15b}$$

with $\alpha = -v/d$ and the recursive relation for polynomials $P_n(\alpha)$ given by [19]

$$P_n = \begin{cases} 1 & n = 0, \\ \alpha & n = 1, \\ (2n-1)\alpha P_{n-1} - (n-1)^2 P_{n-2} & n \ge 2. \end{cases} \tag{15c}$$

By direct differentiation, the approximation to G^F_h is written as

$$G^F_h \approx -2\pi \mathrm{e}^v [Y_1(h) - \mathrm{i} J_1(h)] + 2\sum_{n=0}^{\infty} \mathscr{Q}_n, \tag{16a}$$

where $\mathscr{Q}_n$ are written as

$$\mathscr{Q}_n = \frac{\partial^{n+1}}{\partial h \partial v^n} \left(\frac{1}{d} \right) = -h \frac{Q_n(\alpha)}{d^{n+3}}, \tag{16b}$$

with the recursive relation for polynomials $Q_n(\alpha)$ given by [19]

$$Q_n = \begin{cases} 1 & n = 0, \\ 3\alpha & n = 1, \\ (2n+1)\alpha Q_{n-1} - (n-1)(n+1)Q_{n-2} & n \geq 2. \end{cases} \tag{16c}$$

In the same manner, the approximation to G^F_{hh} is

$$G^F_{hh} \approx -2\pi \mathrm{e}^v \{Y_0(h) - Y_1(h)/h - \mathrm{i}[J_0(h) - J_1(h)/h]\} + 2\sum_{n=0}^{\infty} \mathscr{R}_n, \tag{17a}$$

where $\mathscr{R}_n$ are represented by a combination of $\mathscr{P}_n$ and $\mathscr{Q}_n$ (refer to Appendix B for details):

$$\mathscr{R}_n = \frac{\partial^{n+2}}{\partial h^2 \partial v^n}\left(\frac{1}{d}\right) = -\mathscr{P}_{n+2} - \frac{\mathscr{Q}_n}{h}. \tag{17b}$$

The comparison between approximation via the direct differentiation (17) and the proposed formulation (11a) is considered. To achieve six-decimal accuracy, the series are truncated to $n = 9$ when $d \geq 15$. Fig. 4 depicts the errors due two approximations to the real part of G^F_{hh} as a function of the angle $\arctan(-v/h)$ along an arc $d = 15$. It is observed that the errors due to two approximations are comparable. However, the implementation of the proposed formulation (11a) is straightforward, whereas expression (17b) must be formulated in order to implement the approximation via direct differentiation.

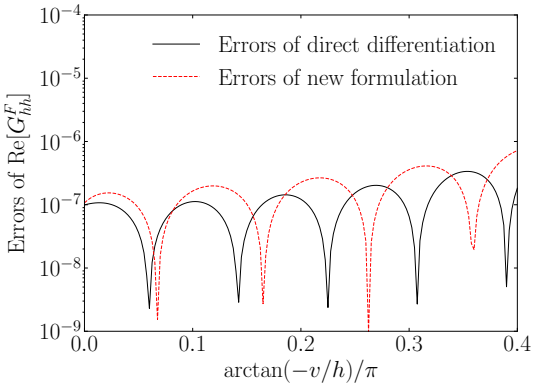

Figure 4: Errors of approximations of G^F_{hh} due to the direct differentiation and the proposed new formulation as a function of the angle $\arctan(-v/h)$ for $d = 15$.

Therefore, the superiority of the proposed formulation over the direct differentiation to approximate the higher-order derivatives of the free-surface term is threefold. Firstly, the proposed formulation could keep the same level of accuracy as G^F and its radial derivative G^F_h, whereas more expansion terms are needed if the direct differentiation is adopted. Secondly, the proposed formulation is straightforward to implement, while additional coefficients/expressions are required to implement the direct differentiation. Lastly, the highly-efficient global approximations given in [11, 12, 13] can be used straightforwardly.

6. Velocity components induced by a constant dipole distribution

In the preceding sections, the evaluation of the free-surface term in the Green function has been studied. As pointed out in [32, 33, 34], however, the Green function itself is not directly useful, and its usefulness is embedded in the BIEs. To implement the hyper-singular BIEs (5) and (6), the velocity components induced by a constant dipole distribution must be calculated, and they are associated with second derivatives of Rankine-source terms featuring hyper-singular. For this reason, this term should be treated separately.

In the constant BEM, the integration of the Rankine-source terms ($-1/r$ and $-1/d$) and its derivatives over a flat panel is usually calculated analytically based on the algorithms given in [35, 36, 37] due to their strongly singular behaviour. It is observed from (11) and (14) that the singularity in the form of $1/d$ as well as its derivatives appear in the derivatives of the free-surface term. Therefore, these terms should also be integrated analytically analogous to the integration of Rankine-source terms. The rest terms are dominated by the logarithmic-type singularity $2\mathrm{e}^v \log(d - v)$ for a small d [6, 7], and they can be integrated over a panel numerically using the Gaussian quadrature rule.

As for the velocity components induced by a distribution of dipole over a flat panel ΔS, they are written as

$$\boldsymbol{u}^S = \nabla_{\boldsymbol{x}} \iint_{\Delta S} \frac{\partial}{\partial n_{\boldsymbol{\xi}}}\left(-\frac{1}{r}\right) \mathrm{d}S. \tag{18}$$

According to [35, 37], a constant dipole distribution can be represented by a closed vortex ring comprising segments of the edge of the panel, and the induced velocity vector can be calculated by the Biot-Savart law which is widely used in the hydrofoil theory [38, 39, 40, 41]. The velocity vector is written as:

$$\boldsymbol{u}^S = \oint_{\Gamma} \frac{\mathrm{d}\boldsymbol{l} \times \boldsymbol{r}}{r^3}, \tag{19}$$

where Γ means the edge of the flat panel. Equation (19) is also applicable when the flow-field point coincides with the centroid of the panel. Suppose that the flat panel consists of N edges, and expression (19) becomes

$$\boldsymbol{u}^S = \sum_{j=1}^{N} \boldsymbol{q}_j. \tag{20}$$

The velocity vector induced by a straight vortex segment $\boldsymbol{l}$ is given by [37]:

$$\boldsymbol{q} = \frac{\boldsymbol{r}_1 \times \boldsymbol{r}_2}{|\boldsymbol{r}_1 \times \boldsymbol{r}_2|^2} \boldsymbol{l} \cdot \left(\frac{\boldsymbol{r}_1}{|\boldsymbol{r}_1|} - \frac{\boldsymbol{r}_2}{|\boldsymbol{r}_2|}\right), \tag{21a}$$

with

$$\boldsymbol{r}_m = (x - \xi_m)\boldsymbol{i} + (y - \eta_m)\boldsymbol{j} + (z - \zeta_m)\boldsymbol{k}, \quad m = 1, 2, \tag{21b}$$

and

$$\boldsymbol{l} = (\xi_2 - \xi_1)\boldsymbol{i} + (\eta_2 - \eta_1)\boldsymbol{j} + (\zeta_2 - \zeta_1)\boldsymbol{k}, \tag{21c}$$

where definitions of $\boldsymbol{r}_1$, $\boldsymbol{r}_2$ and $\boldsymbol{l}$ are illustrated in Fig. 5.

It must be understood that expression (19) only holds for a constant dipole distribution. However, it is noted that the majority of the state-of-the-art commercial and academic potential-flow diffraction/radiation codes are based on constant BEMs, probably due to their simplicity and robustness. In addition, the formulation (19) is generic, thus can be directly applicable in the implementation of either frequency-domain or time-domain diffraction/radiation codes.

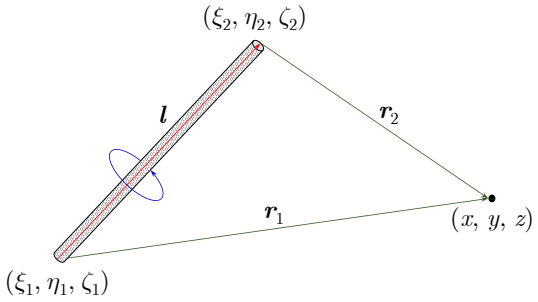

Figure 5: Definition of a vortex segment.

For the velocity components induced by a distribution of mirror dipole above the free surface over a flat panel ΔS, they are written as

$$\boldsymbol{u}^M(x,y,z) = \nabla \iint_{\Delta S} \frac{\partial}{\partial n_q}\left(-\frac{1}{d}\right) \mathrm{d}S, \tag{22}$$

which can be expanded as

$$\boldsymbol{u}^M(x,y,z) = \left\{ \begin{array}{c} \partial_x \\ \partial_y \\ \partial_z \end{array} \right\} \iint_{\Delta S} (n_\xi \partial_\xi + n_\eta \partial_\eta + n_\zeta \partial_\zeta) \times \left(\frac{-1}{\sqrt{h^2 + (z+\zeta)^2}} \right) \mathrm{d}S. \tag{23}$$

Introducing $z' = -z$, expression (22) is rewritten as

$$\boldsymbol{u}^M(x,y,z) = \left\{ \begin{array}{c} \partial_x \\ \partial_y \\ -\partial_{z'} \end{array} \right\} \iint_{\Delta S} (n_\xi \partial_\xi + n_\eta \partial_\eta + n_\zeta \partial_\zeta) \times \left(\frac{-1}{\sqrt{h^2 + (z'-\zeta)^2}} \right) \mathrm{d}S. \tag{24}$$

The integral in (24) is in the form of a dipole distribution in free space, and therefore the velocity components induced by a distribution of mirror dipole are expressed as

$$\left\{ \begin{array}{c} u^M(x,y,z) \\ v^M(x,y,z) \\ w^M(x,y,z) \end{array} \right\} = \left\{ \begin{array}{c} u^S(x,y,-z) \\ v^S(x,y,-z) \\ -w^S(x,y,-z) \end{array} \right\}. \tag{25}$$

7. Illustrative examples

As illustrative examples, the hydrodynamic coefficients of a submerged horizontal circular disc are computed, and both impermeable and perforated plates are considered. The radiation problems for an impermeable plate has been analytically studied by Martin and Farina [30], while Zhao et al. [42] carried out an analytical study of wave diffraction by a perforated plate. Their analytical solutions are used to verify the present computation. In the hyper-singular BIE (5), the normal velocity at the disc surface is written as

$$V_n(\boldsymbol{x}) = n(\boldsymbol{x}) - \mathrm{i}\sigma(\boldsymbol{x})[\phi(\boldsymbol{x})], \tag{26}$$

where σ is defined as $\sigma = k_0 b/(2\pi)$ with $k_0 = \omega^2/g$ and b denoting the wavenumber and a nondimensional parameter associated with the porosity of the plate, respectively [43, 44]. For an impermeable disc, σ is nil. In (26), n represents the normal vector component for the wave radiation problem, and equals to $\partial\phi_0/\partial n$ for the wave diffraction problem where ϕ_0 denotes the potential of incident waves. By solving the hyper-singular integral equation (5), the potential jump across the disc is obtained, and then the hydrodynamic coefficients including added mass, wave-radiation damping and wave exciting force can be calculated.

Due to the presence of sharp edge, the velocity components at the edge are singular in the form of [45, 46]

$$\nabla\phi \sim \varrho^{-1/2} \quad \text{as} \quad \varrho = \sqrt{(h-R)^2 + (z+H)^2} \to 0, \tag{27}$$

where R and H denote the radius and submergence of the disc, respectively. Therefore, very fine elements are needed near the edge to represent strong variation of velocity potential.

7.1. Wave radiation by a heaving impermeable circular plate

The wave radiation by a heaving circular impermeable disc with unit radius $R = 1$ m and shallow submergence $H = 0.1$ m is considered. Fig. 6 depicts the added mass and wave-radiation damping coefficients as a function of $k_0 R$, and nondimensional heave added mass a_{33} and wave-radiation damping b_{33} are nondimensionalised with respect to ρR^3 and $\omega\rho R^3$, respectively. The comparison is made with the analytical solution given by Marin and Farina [30], and good agreement is obtained. In the numerical computation, very fine mesh near the sharp edge is needed. However, this is a common problem in numerical methods when it comes to sharp edges, unless singular functions are included in the local approximations near the sharp edge [46].

7.2. Wave diffraction by a perforated circular disc

Fig. 7 depicts the wave exciting pitch moment experienced by a submerged perforated disc with radius $R = 1$ m and submergence $H = 0.2$ m, and the nondimensional pitch moment is defined as $f_5 = F_5/(\rho g A R^3)$ where A means the amplitude of incident waves. The coefficient associated with the porosity of the disc is $b = 4.0$. The comparison is made with the existing analytical solution by Zhao et al. [42], where a finite water depth $D = 4R$ was considered. Therefore, we don't expect perfect match between our results and that of Zhao et al. [42], since infinite

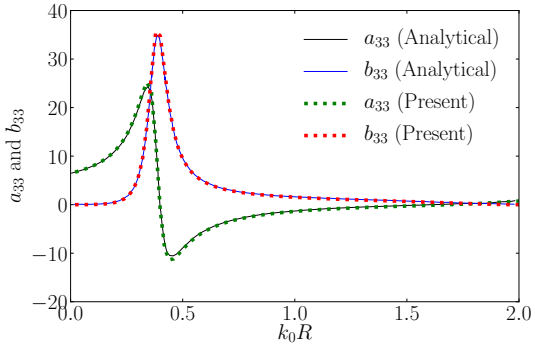

Figure 6: Added mass and wave-radiation damping coefficients of a submerged heaving circular disc for $H/R = 0.1$. H = submergence depth, R = radius of the disc, a_{33} = nondimensional heave added mass, b_{33} = nondimensional wave-radiation damping due to heaving motion, and k_0 = wavenumber.

water depth is assumed throughout this study. Satisfactory agreement is observed for $k_0R \geq 1.5$, whereas slight discrepancy occurred for $k_0R \leq 1.5$ corresponding to the scenario that the wavelength is larger than the water depth indicating that water depth effect matters.

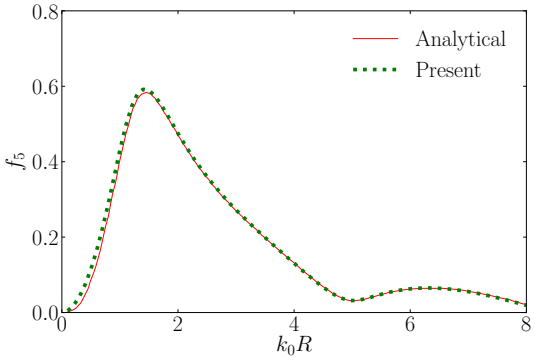

Figure 7: Nondimensional pitch moment of a circular perforated disc for $b = 0.4$ and $H/R = 0.2$. b = nondimensional porosity parameter, H = submergence depth, R = radius of the disc, f_5 = nondimensional pitch moment, and k_0 = wavenumber.

8. Conclusions and future perspectives

The present work is dedicated to circumvent numerical difficulties in the three-dimensional hyper-singular BIEs which meets the requirements of challenging problems, such as: thin plate [23], dissipation surface to suppress unreasonable gap resonance [25, 26], shell structures for wave energy converters [27, 28] and Taylor expansion boundary element method [47, 48]. The contribution of this work is listed below:

1. Higher-order derivatives of the Green function for the wave radiation/diffraction by marine structures are derived. All second derivatives of the free-surface term can be represented by the free-surface term itself G^F and its horizontal radial derivative G_h^F as shown in (10) and (11). Special attention should be paid to the case $h = 0$ due to the zero-over-zero form limit, and the solution to this special case has been given in (14).
2. The comparison with the conventional direct differentiation indicates that the present method to evaluate higher-order derivatives of the free-surface term is superior to the conventional direct differentiation in terms of accuracy and easy implementation.
3. This study enables the evaluation of higher-order derivatives of the free-surface term based on highly-efficient global approximations of G^F and G_h^F given in [11, 12, 13].
4. An alternative method to evaluate the velocity components induced by a uniform dipole distribution, which results in hyper-singular property, is introduced based on the Biot-Savart law, and general explicit expressions are given in (20) and (21).

Despite the present study cannot be straightforwardly generalized to the Green function in finite water depth, yet the recent studies [49, 50] show that the finite-depth Green function contains two terms analogous to the wavenumber integral (8). To this end, this study can still benefit the evaluation of higher-order derivatives of the Green function in finite water depth.

Acknowledgments

The first author is supported by A*STAR Science and Engineering Research Council, Grant Number 172 19 00089 under the Marine & Offshore Strategic Research Programme (M&O SRP). The second author is supported by Independent Research Fund Denmark, Grant Number 0136-00329B.

Appendix A. Derivation of second derivatives of the free-surface term

The integral expressions for G^F and G_h^F are expressed as

$$G^F = -2\int_0^\infty \frac{1}{k-1} e^{kv} J_0(kh)\mathrm{d}k, \tag{A.1a}$$

$$G_h^F = 2\int_0^\infty \frac{k}{k-1} e^{kv} J_1(kh)\mathrm{d}k. \tag{A.1b}$$

Then, the second derivatives G_{hh}^F, G_{hv}^F and G_{vv}^F are respectively written as

$$\begin{aligned} G_{hh}^F =& 2\int_0^\infty \frac{k^2}{k-1} e^{kv}\left[J_0(kh) - \frac{J_1(kh)}{kh}\right]\mathrm{d}k \\ =& 2\int_0^\infty k e^{kv} J_0(kh)\mathrm{d}k + 2\int_0^\infty e^{kv} J_0(kh)\mathrm{d}k \\ &+ 2\int_0^\infty \frac{1}{k-1} e^{kv} J_0(kh)\mathrm{d}k - \frac{G_h^F}{h} \\ =& -\frac{2v}{d^3} + \frac{2}{d} - G^F - \frac{G_h^F}{h}, \end{aligned} \tag{A.2a}$$

$$\begin{aligned} G_{hv}^F =& 2\int_0^\infty \frac{k^2}{k-1} e^{kv} J_1(kh)\mathrm{d}k \\ =& 2\int_0^\infty k e^{kv} J_1(kh)\mathrm{d}k + 2\int_0^\infty \frac{k}{k-1} e^{kv} J_1(kh)\mathrm{d}k \\ =& \frac{2h}{d^3} + G_h^F, \end{aligned}$$

(A.2b)

$$
\begin{aligned}
G^F_{vv} =& -2\fint_0^\infty \frac{k^2}{k-1}\mathrm{e}^{kv}J_0(kh)\mathrm{d}k \\
=& -2\int_0^\infty k\mathrm{e}^{kv}J_0(kh)\mathrm{d}k - 2\int_0^\infty \mathrm{e}^{kv}J_0(kh)\mathrm{d}k \\
& -2\fint_0^\infty \frac{1}{k-1}\mathrm{e}^{kv}J_0(kh)\mathrm{d}k \\
=& \frac{2v}{d^3} - \frac{2}{d} + G^F,
\end{aligned}
\tag{A.2c}
$$

where the relation in (B.1) has been used.

Appendix B. Evaluation of $\mathscr{R}_n$

Evaluations of $\mathscr{R}_n$ are formulated in this appendix. The expression $1/d$ can be expressed in the form of the Laplace transform of the zeroth-order Bessel function of the first kind [51]:

$$
\frac{1}{\sqrt{h^2+v^2}} = \int_0^\infty \mathrm{e}^{kv}J_0(kh)\mathrm{d}k. \tag{B.1}
$$

By definition, $\mathscr{P}_n$, $\mathscr{Q}_n$ and $\mathscr{R}_n$ are written as:

$$
\mathscr{P}_n = \int_0^\infty k^n\mathrm{e}^{kv}J_0(kh)\mathrm{d}k, \tag{B.2a}
$$

$$
\mathscr{Q}_n = \frac{\partial\mathscr{P}_n}{\partial h} = -\int_0^\infty k^{n+1}\mathrm{e}^{kv}J_1(kh)\mathrm{d}k, \tag{B.2b}
$$

$$
\mathscr{R}_n = \frac{\partial^2\mathscr{P}_n}{\partial h^2} = \int_0^\infty k^{n+2}\mathrm{e}^{kv}\left[-J_0(kh) + \frac{J_1(kh)}{kh}\right]\mathrm{d}k. \tag{B.2c}
$$

By comparison, $\mathscr{R}_n$ can be obtained by a combination of $\mathscr{P}_n$ and $\mathscr{Q}_n$

$$
\mathscr{R}_n = -\mathscr{P}_{n+2} - \frac{\mathscr{Q}_n}{h}. \tag{B.3}
$$

References

[1] Faltinsen OM. Sea Loads on Ships and Offshore Structures. Cambridge University Press; 1993.

[2] Molin B. Hydrodynamique des Structures Offshore. Editions Technip; 2002.

[3] Cummins WE. The impulse response function and ship motions. Schiffstechnik, 1962;9(47):101–9.

[4] Ogilvie TF. Recent progress towards the understanding and prediction of ship motions. In: Proceeding of Fifth Symposium on Naval Hydrodynamics, Washington,D.C.: Office of Naval ResearchDepartment of the Navy. 1964, p. 3–128.

[5] Wehausen JV, Laitone EV. Surface waves. Hanbuch der Physik 1960;9:446–778.

[6] Noblesse F. The Green function in the theory of radiation and diffraction of regular water waves by a body. Journal of Engineering Mathematics 1982;16(2):137–69.

[7] Newman JN. Algorithms for the free-surface Green function. Journal of Engineering Mathematics 1985;19(1):57–67.

[8] Telste JG, Noblesse F. Numerical evaluation of the Green function of water-wave radiation and diffraction. Journal of Ship Research 1986;30(2):69–84.

[9] Newman JN. The approximation of free-surface Green functions. In: Martin PA, Wickham GR, editors. Wave Asymptotics; chap. 4. Cambridge, UK: Cambridge University Press; 1992, p. 107–35.

[10] Chen XB. Hydrodynamics in offshore and naval applications. In: Proceeding of the 6th International Conference on Hydrodynamics, Perth, Australia. 2004,.

[11] Wu H, Zhang C, Zhu Y, Li W, Wan D, Noblesse F. A global approximation to the Green function for diffraction radiation of water waves. European Journal of Mechanics - B/Fluids 2017;65(1):54–64.

[12] Liang H, Wu H, Noblesse F. Validation of a global approximation for wave diffraction-radiation in deep water. Applied Ocean Research 2018;74:80–6.

[13] Wu H, Liang H, Noblesse F. Wave component in the Green function for diffraction radiation of regular water waves. Applied Ocean Research 2018;81:72–5.

[14] Delhommeau G. Amélioration des performances des codes de calcul de diffraction-radiation au premier ordre. In: Proceedings of the 2èmes Journées de l'Hydrodynamique, Nantes, France. 1989, p. 69–88.

[15] Ponizy B, Noblesse F, Ba M, Guilbaud M. Numerical evaluation of free-surface Green functions. Journal of Ship Research 1994;38(3):193–202.

[16] Shen Y, Yu D, Duan W, Ling H. Ordinary differential equation algorithms for a frequency-domain water wave Greens function. Journal of Engineering Mathematics 2016;100(1):53–66.

[17] Xie C, Chen X, Clément AH, Babarit A. A new ordinary differential equation for the evaluation of the frequency-domain Green function. Applied Ocean Research 2019;86:239–45.

[18] Newman JN. A simplified derivation of the ordinary differential equations for the free-surface Green functions. Applied Ocean Research 2020;94:101973.

[19] Xie C, Choi Y, Rongère F, Clément AH, Delhommeau G, Babarit A. Comparison of existing methods for the calculation of the infinite water depth free-surface Green function for the wave–structure interaction problem. Applied Ocean Research 2018;81:150–63.

[20] Shao YL, You J, Glomnes EB. Stochastic linearization and its application in motion analysis of cylindrical floating structure with bilge boxes. In: Proceeding of the 35th International Conference on Ocean, Offshore and Arctic Engineering, Busan, Korea. American Society of Mechanical Engineers Digital Collection; 2016,.

[21] Xiang X, Svangstu E, Nedrebø Ø, Jakobsen B, Eidem ME, Larsen PN, et al. Viscous damping modelling of floating bridge pontoons with heaving skirt and its impact on bridge girder bending moments. In: International Conference on Offshore Mechanics and Arctic Engineering. American Society of Mechanical Engineers; 2017,.

[22] Shao YL, Xiang X, Liu J. Numerical investigation of wave-frequency pontoon responses of a floating bridge based on model test results. In: Proceeding of the 38th International Conference on Ocean, Offshore and Arctic Engineering, Glasgow, Scotland. American Society of Mechanical Engineers Digital Collection; 2019,.

[23] Teng B, Huang J. Examination of extraordinary transmission of waves propagation through gaps of vertical thin barriers in channels by a hypersingular boundary element method. China Ocean Engineering 2019;33(5):509–21.

[24] An S, Faltinsen OM. An experimental and numerical study of heave added mass and damping of horizontally submerged and perforated rectangular plates. Journal of Fluids and Structures 2013;39:87–101.

[25] Feng X, Chen XB, Dias F. A potential flow model with viscous dissipation based on a modified boundary element method. Engineering Analysis with Boundary Elements 2018;97:1–15.

[26] Lee CH, Zhu X. Application of hyper-singular integral equations for a simplified model of viscous dissipation. In: Proceeding of the 28th International Ocean and Polar Engineering Conference, Sapporo, Japan. International Society of Offshore and Polar Engineers; 2018,.

[27] Renzi E, Dias F. Resonant behaviour of an oscillating wave energy converter in a channel. Journal of Fluid Mechanics 2012;701:482–510.

[28] Hariri Nokob M, Yeung RW. Diffraction and radiation loads on

open cylinders of thin and arbitrary shapes. Journal of Fluid Mechanics 2015;772:649–77.
[29] Liang H, Ouled Housseine C, Chen XB, Shao Y. Efficient methods free of irregular frequencies in wave and solid/porous structure interactions. Journal of Fluids and Structures 2020;98:103130.
[30] Martin PA, Farina L. Radiation of water waves by a heaving submerged horizontal disc. Journal of Fluid Mechanics 1997;337:365–79.
[31] Abramowitz M, Stegun IA. Handbook of Mathematical Functions: with Formulas, Graphs, and Mathematical Tables. 55; National Bureau of Standards; 1964.
[32] Chen XB, Liang H. Wavy properties and analytical modeling of free-surface flows in the development of the multi-domain method. Journal of Hydrodynamics 2016;28(6):971–6.
[33] Liang H, Chen XB. A new multi-domain method based on an analytical control surface for linear and second-order mean drift wave loads on floating bodies. Journal of Computational Physics 2017;347:506–32.
[34] Chen XB, Liang H, Li RP, Feng XY. Ship seakeeping hydrodynamics by multi-domain method. In: Proceedings of 32nd Symposium on Naval hydrodynamics, Hamburg, Germany. 2018,.
[35] Hess JL. Calculation of potential flow about arbitrary three-dimensional lifting bodies. Tech. Rep. MDC J5679-01; 1972.
[36] Newman JN. Distributions of sources and normal dipoles over a quadrilateral panel. Journal of Engineering Mathematics 1986;20(2):113–26.
[37] Katz J, Plotkin A. Low-speed aerodynamics. 2 ed.; Cambridge University Press; 2001.
[38] Faltinsen OM. Hydrodynamics of High-Speed Marine Vehicles. Cambridge University Press; 2005.
[39] Liang H, Sun L, Zong Z, Zhou L, Zou L. Analytical modelling for a three-dimensional hydrofoil with winglets operating beneath a free surface. Applied Mathematical Modelling 2013;37(5):2679–701.
[40] Liang H, Zong Z, Sun L, Zou L, Zhou L, Zhao YJ, et al. Generalized Weissingers L-method for prediction of curved wings operating above a free surface in subsonic flow. Journal of Engineering Mathematics 2013;83(1):109–29.
[41] Liang H, Zong Z, Zou L. Nonlinear lifting theory for unsteady WIG in proximity to incident water waves. Part 2: Three-dimension. Applied Ocean Research 2013;43:88–98.
[42] Zhao F, Chen Y, Wan R, Huang L, Sun P, Bao W. Interactions of horizontal circular porous plates with waves. In: Proceeding of the 25th International Ocean and Polar Engineering Conference, Hawaii, USA. International Society of Offshore and Polar Engineers; 2015,.
[43] Chwang AT. A porous-wavemaker theory. Journal of Fluid Mechanics 1983;132:395–406.
[44] Zhao F, Bao W, Kinoshita T, Itakura H. Theoretical and experimental study on a porous cylinder floating in waves. Journal of Offshore Mechanics and Arctic Engineering 2011;133(1):011301.
[45] Newman JN. Marine Hydrodynamics. Massachusetts Institute of Technology Press; 1977.
[46] Liang H, Faltinsen OM, Shao YL. Application of a 2D harmonic polynomial cell (HPC) method to singular flows and lifting problems. Applied Ocean Research 2015;53:75–90.
[47] Duan WY, Chen JK, Zhao BB. Second-order Taylor Expansion Boundary Element Method for the second-order wave diffraction problem. Engineering Analysis with Boundary Elements 2015;58:140–50.
[48] Duan WY, Chen JK, Zhao BB. Second-order Taylor Expansion Boundary Element Method for the second-order wave radiation problem. Applied ocean research 2015;52:12–26.
[49] Liu Y, Yoshida S, Hu C, Sueyoshi M, Sun L, Gao J, et al. A reliable open-source package for performance evaluation of floating renewable energy systems in coastal and offshore regions. Energy Conversion and Management 2018;174:516–36.
[50] Mackay EBL. Consistent expressions for the free-surface Green function in finite water depth. Applied Ocean Research 2019;93:101965.
[51] Watson GN. A treatise on the theory of Bessel functions. Cambridge University Press; 1995.